

DOUBLE ASYMPTOTIC SCALING AT HERA

Richard D. Ball* and Stefano Forte†

*Theory Division, CERN,
CH-1211 Genève 23, Switzerland.*

Abstract

Perturbative QCD predicts that at sufficiently large Q^2 and small x nucleon structure functions should exhibit scaling in the two variables $\sqrt{\ln \frac{1}{x} \ln \ln Q^2}$ and $\sqrt{\ln \frac{1}{x} / \ln \ln Q^2}$, provided only that the small- x behaviour of the input to the perturbative QCD evolution is sufficiently soft. We derive these asymptotic results by writing the gluonic Altarelli–Parisi equation at small x as a two-dimensional wave equation, which propagates the gluon distribution from its boundaries into the asymptotic region. We then show that the existing experimental data on $F_2^p(x, Q^2)$ from HERA provide a remarkable confirmation of both of these scaling predictions. The ‘hard’ pomeron, which does not scale, is thereby excluded by more than three standard deviations; only a very small admixture of it is permitted by the data. We propose that existing and future data from HERA should be binned in the two scaling variables, in order to facilitate the search for small scaling violations.

Submitted to: *Physics Letters B*

CERN-TH.7265/94

May 1994

* On leave from a Royal Society University Research Fellowship.

† On leave from INFN, Sezione di Torino, Italy.

The main evidence for perturbative QCD in deep inelastic scattering at large x comes from the observation of small violations of Bjorken scaling [1] in the structure function $F_2(x;t)$ in the Bjorken limit of large $t \equiv \ln Q^2/\Lambda^2$ at fixed x . These scaling violations may be accurately predicted using the operator product expansion [2] or equivalently the Altarelli–Parisi equations [3]. In this letter we will show that in the double limit of large t and small x perturbative QCD also makes definite scaling predictions, provided only that the gluon distribution at scales of order 1 GeV is reasonably soft at small x (i.e. that the pomeron intercept is close to one). The appropriate scaling variables are the geometric mean $\sigma \simeq \sqrt{\ln \frac{1}{x} \ln t}$ and the ratio $\rho \simeq \sqrt{\ln \frac{1}{x} / \ln t}$; the gluon distribution then scales asymptotically in both σ and ρ in the double limit of large σ at fixed ρ and large ρ at fixed σ . These simple predictions, which are asymptotically parameter free up to an overall normalization factor, may be directly tested by comparison with experiment. Indeed, we will show that recent data from HERA [4,5] are in remarkable agreement with this asymptotic behaviour. Furthermore, since the double asymptotic scaling would necessarily be spoiled if the pomeron were hard, we will be able to use it as a means to discriminate experimentally between soft and hard pomerons.

Before actually proceeding to the comparison of double asymptotic scaling behaviour with the data, we first derive it in a simple but, we believe, instructive way by reducing the singlet Altarelli–Parisi equations at small- x and large t to a wave-like equation for the gluon distribution, which may be solved exactly. We then derive the asymptotic form of this solution for large values of the scaling variables σ and ρ , and different classes of boundary conditions, namely ‘soft’ and ‘hard’. We explain in what sense solutions with soft boundary conditions exhibit double asymptotic scaling, establish the kinematic region in which this scaling behaviour sets in, and show the way in which it is corrupted if the boundary conditions are ‘hard’. We derive a simple relation between F_2 and the gluon distribution in the asymptotic region, and finally proceed to a direct comparison with the experimental data.

We will be concerned specifically with the singlet contribution to the proton structure function

$$\begin{aligned}
 F_2^p(x;t) &= \frac{5}{18} xq(x;t) + F_2^{NS}(x;t) \\
 q(x;t) &\equiv \sum_{i=1}^{n_f} (q_i(x;t) + \bar{q}_i(x;t)),
 \end{aligned}
 \tag{1}$$

where n_f is the number of active flavours. At small enough x the nonsinglet contribution $F_2^{NS}(x;t)$ is negligible and can be ignored. At small x and large t the singlet quark

distribution $q(x; t)$ is essentially driven by the generic instability of the gluon distribution $g(x; t)$; determining the latter thus allows us to compute F_2^p in this kinematic region.

To see how this works, consider the singlet Altarelli–Parisi equations [3], which describe perturbative evolution of $g(x; t)$ and $q(x; t)$ in the kinematical region displayed in fig. 1:

$$\begin{aligned}\frac{\partial}{\partial t}g(x; t) &= \frac{\alpha_s(t)}{2\pi} \int_x^1 \frac{dy}{y} [P_{gg}(\frac{x}{y})g(y; t) + P_{gq}(\frac{x}{y})q(y; t)], \\ \frac{\partial}{\partial t}q(x; t) &= \frac{\alpha_s(t)}{2\pi} \int_x^1 \frac{dy}{y} [2n_f P_{qg}(\frac{x}{y})g(y; t) + P_{qq}(\frac{x}{y})q(y; t)],\end{aligned}\tag{2}$$

where $\alpha_s(t) = \frac{4\pi}{\beta_0 t} + O(\frac{1}{t^2})$, $\beta_0 = 11 - \frac{2}{3}n_f$. Solving these equations sums up all leading logarithms of the form $\alpha_s^m \ln^m Q^2 \ln^n \frac{1}{x}$ with $n \leq m$; terms with fewer powers of $\ln Q^2$ should be negligible if t is large enough for perturbation theory to be trusted ($t > t_0$ say, where $\alpha_s(t_0) \ll 1$).

Now evolution at small x ($x < x_0$, say) will be dominated by the lowest moments of the splitting functions; this may be demonstrated explicitly by taking the Mellin transform of the evolution equations (2), solving them, and then using a saddle-point evaluation of the inverse Mellin transform of the solution[6,7]. In practice, this is equivalent to expanding the Mellin transform of the one loop splitting functions about their largest singularity in moment space (which is when the moment variable $n \rightarrow 0$) and discarding terms which vanish as $n \rightarrow 0$ [8,9]. Inverting the transform again, this leads to the approximate form of the splitting functions

$$\begin{aligned}P_{gg}(z) &\approx \frac{6}{z} - (\frac{11}{2} + \frac{n_f}{3})\delta(1-z), & P_{gq}(z) &\approx \frac{8}{3z} - 2\delta(1-z), \\ P_{qg}(z) &\approx \frac{1}{3}\delta(1-z), & P_{qq}(z) &\approx 0.\end{aligned}\tag{3}$$

When substituted into (2), the terms in (3) which go as z^{-1} will sum all the double logarithms, while the terms proportional to $\delta(1-z)$ will approximately sum the remaining single logarithms¹; in terms of ladder diagrams, the former terms account for rungs which are strongly ordered in both x and t , the latter for rungs which are only strongly ordered in t . If only the former terms were retained one would get the so-called double-leading logarithm approximation.

¹ This approximation could be refined by keeping higher powers of n in the Mellin transform of the splitting function. This leads to further terms in (3) involving derivatives of the delta function.

Defining for convenience two new variables

$$\xi \equiv \ln\left(\frac{x_0}{x}\right), \quad \zeta \equiv \ln\left(\frac{t}{t_0}\right) = \ln\left(\frac{\ln Q^2/\Lambda^2}{\ln Q_0^2/\Lambda^2}\right) \quad (4)$$

(so that at $x = x_0$ $\xi = 0$, and at $t = t_0$ $\zeta = 0$), and writing

$$G(\xi, \zeta) \equiv xg(x; t), \quad Q(\xi, \zeta) \equiv xq(x; t) = \sum_i x(q_i(x; t) + \bar{q}_i(x; t)), \quad (5)$$

then substituting (3) into (2), and differentiating the first equation with respect to ξ , the singlet evolution equations assume the simple form

$$\frac{\partial^2}{\partial \xi \partial \zeta} G(\xi, \zeta) + \delta' \frac{\partial}{\partial \xi} G(\xi, \zeta) - \gamma^2 G(\xi, \zeta) = \frac{4\gamma^2}{9} Q(\xi, \zeta) - \frac{\gamma^2}{3} \frac{\partial}{\partial \xi} Q(\xi, \zeta), \quad (6)$$

$$\frac{\partial}{\partial \zeta} Q(\xi, \zeta) = \frac{n_f \gamma^2}{9} G(\xi, \zeta), \quad (7)$$

where $\gamma \equiv \sqrt{12/\beta_0}$ and $\delta' \equiv (11 + \frac{2n_f}{3})/\beta_0$. These equations should be valid throughout the first quadrant of the (ξ, ζ) plane (fig. 2), outside the multiple rescattering region $\xi \gg e^{2\zeta}$ [9], up to corrections of order $x_0 e^{-\xi}$ and $\alpha_s(t_0) e^{-\zeta}$.²

The inhomogeneous term on the right hand side of (6) is negligible due to its small coefficient and may be dropped. However, this is not necessary: if the matrix of splitting functions is diagonalized before the Mellin inversion,³ this term is in effect absorbed into a small shift in δ' , which becomes $\delta \equiv (11 + \frac{2n_f}{27})/\beta_0$. The gluon evolution equation (6) then becomes homogeneous,

$$\left[\frac{\partial^2}{\partial \xi \partial \zeta} + \delta \frac{\partial}{\partial \xi} - \gamma^2 \right] G(\xi, \zeta) = 0, \quad (8)$$

while the quark evolution equation (7) remains unchanged (up to subleading corrections).

² Corrections to the expansions (3) of the one loop splitting functions will lead to contributions to the parton distributions which are suppressed by powers of ρ^{-1} (where ρ is as defined in (11) below). Furthermore it may be shown by explicit computation that the two loop corrections to (3) have little effect on the final form of F_2 provided $\sigma \gtrsim 1$ and $1 \lesssim \rho \lesssim 3$. However for $n \lesssim 0.35$, which in practice means $\rho \gtrsim 3$, there are indications that perturbation theory may begin to break down[10].

³ Although in general the diagonalization introduces an extra singularity (a branch cut) this is not a problem here since we expand about $n = 0$.

We next make the essentially trivial observation that (8) is in fact a two dimensional wave equation, with ‘time’ $\frac{1}{2}(\xi + \zeta)$ and ‘space’ $\frac{1}{2}(\xi - \zeta)$. This allows us to immediately infer many useful properties of its solutions, and thus deduce directly many well-known qualitative features of parton evolution. In particular:

- (i) The equation is essentially symmetrical in ξ and ζ , so the gluon distribution $xg(x; t)$ evolves (‘propagates’) equally in both x and t (up to the (small) asymmetry induced by the ‘damping’ term proportional to δ). Any further asymmetry in ξ and ζ must thus come from the boundary conditions.
- (ii) The propagation is ‘timelike’, into the forward ‘light-cone’ at the origin $(\xi, \zeta) = (0, 0)$, along the ‘characteristics’ $\xi = \text{constant}$ and $\zeta = \text{constant}$ (see fig. 2).
- (iii) At a given point (ξ, ζ) , $G(\xi, \zeta)$ depends only on the boundary conditions contained within the backward light cone formed by the two characteristics through (ξ, ζ) fig. 2. This means that to calculate $xg(x; t)$ it is unnecessary to know what happens at smaller values of x or larger values of t .
- (iv) Because the equation is linear, contributions to $G(\xi, \zeta)$ from different parts of the boundaries are simply added together.
- (v) Since the ‘mass’ term is negative ($\gamma^2 > 0$), the propagation is ‘tachyonic’; this means that $G(\xi, \zeta)$ is unstable, growing exponentially rather than oscillating.
- (vi) Since $\delta > 0$ the damping term ensures that, at fixed ξ $G(\xi, \zeta)$ eventually falls with increasing ζ .

Setting $G(\xi, \zeta)$ along two characteristics (for example $\xi = 0$ and $\zeta = 0$) gives a well-posed problem (the ‘characteristic Goursat problem’ [11]) provided only that the boundary conditions are compatible at the point where the boundaries meet. Since the Green’s function for the wave operator (8) may be expressed in terms of the Bessel function

$$I_0(z) \equiv \sum_0^{\infty} \frac{\left(\frac{1}{4}z^2\right)^n}{(n!)^2} \underset{z \rightarrow \infty}{\sim} \frac{1}{\sqrt{2\pi z}} e^z \left(1 + O\left(\frac{1}{z}\right)\right), \quad (9)$$

the general solution to this problem is simply

$$\begin{aligned} G(\xi, \zeta) = & I_0(2\gamma\sqrt{\xi\zeta})e^{-\delta\zeta}G(0, 0) + \int_0^\xi d\xi' I_0(2\gamma\sqrt{(\xi - \xi')\zeta})e^{-\delta\zeta} \frac{\partial}{\partial \xi'} G(\xi', 0) \\ & + \int_0^\zeta d\zeta' I_0(2\gamma\sqrt{\xi(\zeta - \zeta')})e^{\delta(\zeta' - \zeta)} \left(\frac{\partial}{\partial \zeta'} G(0, \zeta') + \delta G(0, \zeta') \right). \end{aligned} \quad (10)$$

The asymptotic behaviour of G away from the boundaries will depend in general on whether the boundary conditions are compact or noncompact, i.e., on whether the starting

distributions are soft or hard at large ξ on the $\zeta = 0$ boundary and large ζ on the $\xi = 0$ boundary. Due to the linearity property, we can consider each boundary separately, and then add the various contributions. We consider first the simplest case in which both boundary conditions are soft, so $g(x; t_0) \sim x^{-1}$ as $x \rightarrow 0$ (i.e. $G(\xi, 0) \sim \text{const.}$ as $\xi \rightarrow \infty$), the traditional behaviour inferred from the intercept of the ‘soft’ pomeron [12], while $g(x_0; t) \sim t^{-\delta}$ as $t \rightarrow \infty$ (i.e. $G(0, \zeta) \sim e^{-\delta\zeta}$ as $\zeta \rightarrow \infty$). Since in this case ‘waves’ are only generated close to the origin, far from the origin we may determine the behaviour of the solution (10) by means of a multipole expansion, i.e., expanding the Bessel functions under the integrals in eq.(10) in powers of $\frac{\xi'}{\xi}$ and $\frac{\zeta'}{\zeta}$ respectively. Defining the new scaling variables

$$\sigma \equiv \sqrt{\xi\zeta} = \sqrt{\ln \frac{x_0}{x} \ln \frac{t}{t_0}}, \quad \rho \equiv \sqrt{\frac{\xi}{\zeta}} = \sqrt{\frac{\ln \frac{x_0}{x}}{\ln \frac{t}{t_0}}}, \quad (11)$$

and considering the limit $\sigma \rightarrow \infty$ at fixed (but reasonably large) ρ (see fig. 2),⁴ we then find asymptotically the generic behaviour

$$\begin{aligned} G(\sigma, \rho) &\underset{\sigma \rightarrow \infty}{\sim} I_0(2\gamma\sigma) e^{-\delta(\sigma/\rho)} \left\{ G(0, 0) \right. \\ &\quad \left. + \int_0^\xi d\xi' \frac{\partial G}{\partial \xi'} e^{-(\gamma/\rho)\xi'} + \int_0^\zeta d\zeta' \left(\frac{\partial G}{\partial \zeta'} + \delta G \right) e^{(\delta-\gamma\rho)\zeta'} + O\left(\frac{1}{\sigma}\right) \right\} \\ &\underset{\sigma \rightarrow \infty}{\sim} \mathcal{N} f_g(y) \frac{1}{\sqrt{4\pi\gamma\sigma}} \exp \left\{ 2\gamma\sigma - \delta\left(\frac{\sigma}{\rho}\right) \right\} \left(1 + O\left(\frac{1}{\sigma}\right) \right). \end{aligned} \quad (12)$$

where $y \equiv \gamma/\rho$, and in the second line we used the asymptotic behaviour (9) of the Bessel function. The normalization factor \mathcal{N} is just that of the boundary condition⁵, while $f_g(0) = 1$, but $f_g(y)$ will depend on the particular details of the boundary condition, while being generally rather smooth.⁶ The asymptotic behaviour (12) is thus, as expected, independent of the detailed form of boundary condition, up to corrections of order $1/\rho$,

⁴ More precisely, we consider the limit $\sigma \rightarrow \infty$ along any curve such that also $\rho \rightarrow \infty$, such as for example the curve $\xi \propto \zeta^{1+\epsilon}$ with $\epsilon > 0$.

⁵ The boundary condition $g(x; t_0)$ will be normalized so that the second moment (the gluon momentum fraction) is unity; the boundary condition $g(x_0, t)$ is then normalized by continuity at (x_0, t_0) . When comparing to the data, the overall normalization will thus give the gluon momentum fraction.

⁶ For example if $xg(x; t_0) = \mathcal{N}(1-x)^\beta$, $x_0g(x_0; t) = \mathcal{N}(1-x_0)^\beta \left(\frac{t}{t_0}\right)^{-\delta}$, then $f_g(y) = (1-x_0)^\beta + \beta x_0 \sum_{n=0}^{\beta-1} \frac{(\beta-1)!}{n!(\beta-1-n)!} \frac{(-x_0)^n}{1+n+y} \sim 1 - \beta x_0 \frac{y}{1+y} + O(x_0^2)$ as $x_0 \rightarrow 0$.

which are anyway of the same order as corrections due to the terms lost by the truncation (3) of the expansion of the splitting functions.

If instead the boundary conditions are noncompact, it is not difficult to see from (10) that the form of $G(\xi, \zeta)$ on the boundary will tend to persist into the interior of the (ξ, ζ) plane; the asymptotic behaviour close to the boundary will then not be universal, but depend on the particular boundary conditions adopted. Consider for example $xg(x; t_0) \sim \mathcal{N}'x^{-\lambda}$, (phenomenologically $\lambda \simeq 0.08$ [13]). Then if $\rho > \frac{\gamma}{\lambda}$, the first boundary integral in eq.(10) is dominated by a nontrivial saddle-point, and gives the asymptotic behaviour

$$G(\sigma, \rho) \underset{\sigma \rightarrow \infty}{\sim} \mathcal{N}' \exp \left\{ \lambda \sigma \rho + \left(\frac{\gamma^2}{\lambda} - \delta \right) \left(\frac{\sigma}{\rho} \right) \right\} \left(1 + O\left(\frac{1}{\sigma}\right) \right), \quad (13)$$

to be added to (12). Very close to the boundary ($\rho \gtrsim 15$) the power-like growth at small x is thus preserved by the evolution to $t > t_0$. However further away from the boundary, in the region $\rho \lesssim \frac{\gamma}{\lambda}$ the more gentle growth (12) is unchanged, modulo a slight increase in \mathcal{N} . Similarly, if the boundary condition on the other boundary is hard (say $G(0, \zeta) \sim e^{-\delta' \zeta}$ as $\zeta \rightarrow \infty$, with $0 \lesssim \delta' < \delta$), this too will propagate into the region $\rho \lesssim \frac{(\delta - \delta')}{\gamma}$, in effect reducing the value of δ close to the boundary. Again away from the boundary the universal behaviour (12) is unaffected.

Thus with only the rather conservative assumption of reasonably soft boundary conditions (i.e. for sufficiently small λ and δ') perturbative QCD predicts a universal growth (12) in the gluon structure function at large t and small x , faster than any power of $\ln \frac{1}{x}$ but slower than any inverse power of x . This means that away from the boundaries perturbative QCD allows us to predict in a parameter-free way (i.e. independently of the precise form of the boundary conditions) the asymptotic behaviour of the gluon distribution, and hence (as we will see below) of the F_2 structure function, throughout a very large region of the (x, t) plane fig. 1. Although it has been known now for twenty years [6], hitherto this remarkable consequence of the perturbative QCD evolution equations seems not to have been taken very seriously. Here we hope to remedy this.

We begin by noting that the universal asymptotic behaviour (12) actually implies scaling in both σ and ρ : $\ln G(\sigma, \rho)$ at fixed ρ is asymptotically a linear function of σ , with slope independent of ρ (up to terms which vanish as $1/\rho$), while at fixed σ it is asymptotically a flat function of ρ . In other words $\sigma^{-1} \ln G(\sigma, \rho)$ is asymptotically independent of both σ and ρ , up to corrections which vanish as $1/\sigma$ and $1/\rho$. This ‘double asymptotic scaling’ is a direct result of two generic properties of wave propagation from compact boundaries:

at large distances from the boundaries, the details of the boundary conditions are washed out (σ scaling)⁷, and, apart from the damping term (which is asymptotically subleading) the propagation is isotropic (ρ scaling).

This double scaling property is peculiar to the universal behaviour (12) derived from reasonably soft boundary conditions; instead, if one of the boundary conditions is very hard, its influence will spread into a large part of the (ξ, ζ) plane, spoiling both ρ and σ scaling in this region in a way that will depend explicitly on the particular form of the hard boundary condition. For example consider the Lipatov ‘hard’ pomeron[15], which grows as a power of $\frac{1}{x}$ as $x \rightarrow 0$ at fixed t : $xg(x; t_0) \sim \mathcal{N}'x^{-\lambda}$, with $\lambda \lesssim \frac{12\ln 2}{\pi}\alpha_s(t_0) \approx \frac{1}{2}$. This behaviour is supposed to be valid at some intermediate t : it is obtained by summing leading logarithms of the form $\alpha_s^n \ln^n \frac{1}{x}$, terms containing powers of $\ln Q^2$ being ignored; t must be small, but not so small that $\alpha_s(t)$ is too large. It will thus serve as a boundary condition for Altarelli–Parisi evolution into the region $t > t_0$. It will then lead to power-like growth of the form (13) throughout the region $\rho \gtrsim \frac{\gamma}{\lambda}$, which must be *added* to the weaker growth (12) over which it will dominate at large ρ . Although the structure function still grows at small x , it now increases so strongly that double scaling is spoiled.

In what remains of this letter we will compare the double asymptotic scaling prediction (12) with all the available small- x data from the two HERA experiments[4,5], to see whether it is supported empirically, or whether there is instead evidence for other less conventional physics (and in particular the ‘hard’ pomeron) at small- x . Firstly we must establish that there are data in the asymptotic region where double scaling might apply. We thus begin by examining the approach to asymptopia as the general solution (10) evolves away from the boundaries. We choose $x_0 = 0.1$, which should be sufficiently small for (3) to be a good approximation. The starting scale is chosen as $Q_0 = 1\text{GeV}$: not so small that perturbative evolution has broken down, but sufficiently small that the behaviour at small x is given by a nonperturbative boundary condition (or, in the case of the hard pomeron, sufficiently small that logarithms of Q_0^2 may be reasonably ignored).

In fig. 3 we display a contour plot of $G(\xi, \zeta)$ computed from the solution (10) with, for definiteness, the soft boundary condition $G(\xi, 0) = \mathcal{N}(1 - x_0e^{-\xi})^9$ compared with the solution computed from the hard boundary condition $G(\xi, 0) = \mathcal{N}'x_0^{-1/2}e^{\xi/2}(1 - x_0e^{-\xi})^9$.

⁷ The position of the boundaries is also unimportant asymptotically, so even if t_0 is taken to be very small the same generic behaviour will be found at small x and large t ; as we will see, this is sufficient to explain the success of the predictions of ref.[14].

On the $\xi = 0$ boundary we take in both cases $G(0, \zeta) = G(0, 0)$ as (approximately) required empirically when $x_0 = 0.1$. The plots clearly show that the asymptotic behaviour is attained very rapidly in the soft case, around $\sigma \sim 1$; the damping term and the propagation from the lower boundary distort the curves somewhat at small values of ρ , as expected. In the hard case the asymptotic behaviour (13) clearly holds only for large $\rho \gtrsim 3$, while in most of the rest of the region the full solution is a compromise between the two sorts of behaviour. In practice, this means that in much of the HERA kinematic range the evolved hard solution is actually rather similar to the unevolved boundary condition imposed at $\zeta = 0$.

It is now clear that, because almost all of the HERA data (and even some of the older NMC data) lie in the region $\sigma \in [1, 2]$, $\rho \in [1, 3]$, well inside the asymptotic kinematic regime of the soft solution, the universal behaviour (12) should be easily tested, while the hard behaviour should be easily distinguished from it. This is demonstrated explicitly in fig. 4 where we compare the scaling expected from the soft pomeron boundary condition with the hard pomeron prediction (with $\lambda = \frac{1}{2}$). Not only does the hard pomeron generally lead to more gluons in any given range of x , but the number rises rather more steeply at smaller values of x . Thus at fixed ρ (fig. 4i), even though $\ln G(\sigma, \rho)$ is in both cases an (approximately) linear function of σ in the hard case its slope gets steeper for larger values of ρ , while in the scaling case it is universal. Correspondingly at fixed σ , in the soft case $G(\sigma, \rho)$ becomes flat as ρ grows, while in the hard case it rises rather rapidly. This is best exhibited by first performing a simple rescaling of $G(\sigma, \rho)$, by a factor

$$R_G(\sigma, \rho) = \exp(-2\gamma\sigma + \delta(\sigma/\rho) + \frac{1}{2} \ln \sigma), \quad (14)$$

so that the curves with different values of σ lie on top of one another (fig. 4ii). Besides showing the clear distinction to be made between the predictions derived from soft and hard boundary conditions, these plots also confirm that for compact boundary conditions, the asymptotic double scaling regime is indeed reached rather rapidly, at moderately small values of σ and ρ .

Before coming finally to a direct comparison of this predicted behaviour to the data [4,5] we must still relate the calculated gluon distribution to the proton structure function F_2^p measured in the experiments. This is actually rather simple at small x and large t , since all that is necessary is to integrate (7):

$$F_2^p = \frac{5}{18} Q(\xi, \zeta) = \frac{5}{18} Q(\xi, 0) + \frac{5n_f}{162} \gamma^2 \int_0^\zeta d\zeta' G(\xi, \zeta'). \quad (15)$$

With compact boundary conditions, the asymptotic form of F_2^p may then be deduced directly from that of G , by substituting (12) into (15), to give (whenever $\rho > \delta/\gamma$)

$$F_2^p \underset{\sigma \rightarrow \infty}{\sim} \frac{5n_f}{162} y f_q(y) G(\sigma, \rho) \left(1 + O\left(\frac{1}{\sigma}\right)\right), \quad (16)$$

where again $y = \frac{\gamma}{\rho}$, and $f_q(y) \rightarrow 1$ as $y \rightarrow 0$.⁸ A similar relation holds for the asymptotic behaviour (13), but with $y = \lambda$ when $\rho > \frac{\gamma}{\lambda}$. So we can actually use (16) as a good approximation throughout the asymptotic region for any type of boundary condition if we set $y = \sqrt{(\gamma/\rho)^2 + \lambda^2}$. Apart from the subasymptotic factor of γ/ρ the asymptotic growth of the gluon distribution drives a similar growth of the singlet quark distribution, and thus of the structure function F_2^p .

Using (16) to determine a slightly different rescaling factor

$$R_F(\sigma, \rho) = \left[\frac{5n_f}{162} \frac{\gamma}{\rho} \right]^{-1} R_G(\sigma, \rho). \quad (17)$$

we may thus compare the σ and ρ scaling plots fig. 4 to all the available data from ZEUS [4] and H1 [5]. The result is shown in fig. 5. It should be immediately apparent that the agreement with the asymptotic behaviour (12) derived from the soft pomeron boundary condition at t_0 is remarkably good, especially when it is remembered that the asymptotic prediction is parameter free, apart from the precise value of the normalization. The hard pomeron boundary condition on the other hand gives results which are a long way from the data, even when its normalization is reduced. Furthermore, the σ plot provides a nontrivial test of perturbative QCD, since the fitted slope agrees very well with the computed one. Also included in fig. 5i are the data from the NMC collaboration [16]; remarkably those which fall within the asymptotic region agree very well with the line fitted to the HERA data alone, despite their much smaller errors.

We may assess quantitatively the quality of the fit of the predictions to the HERA data by computing the χ^2 of the hard and soft structure functions $(F_2^p)^{\text{soft}}$ and $(F_2^p)^{\text{hard}}$ (obtained using (16) from the gluon distributions displayed in fig. 3a) and b) respectively),

⁸ In fact the function f_q may be determined by integrating the second Altarelli–Parisi equation (2) with the second term set to zero (since its contribution is subasymptotic) and $P_{qg}(z) = \frac{1}{2} [z^2 + (1-z)^2]$; this gives $f_q(y) = \left(1 - \frac{\delta}{\gamma^2} y\right)^{-1} \frac{3(4+3y+y^2)}{2(1+y)(2+y)(3+y)}$. Since we already have a similar uncertainty from f_g in (12), due both to our small x approximation (8) to the gluon evolution equation and ignorance of the boundary conditions, this result will not be used here, though it may be useful for extracting the gluon distribution directly from the data.

	N_s	N_h	χ^2
a)	0.33 ± 0.01	0	18 (52)
b)	0	0.14 ± 0.01	114 (282)
a)+b)	0.31 ± 0.03	0.01 ± 0.01	17 (50)
c)	0	0.36 ± 0.01	121 (285)
a)+c)	0.30 ± 0.05	0.03 ± 0.01	17 (49)
d)	0	0.17 ± 0.01	67 (168)
a)+d)	0.30 ± 0.05	0.02 ± 0.01	17 (50)

Table: The fitted normalizations N_s and N_h and the associated χ^2 s (those in parenthesis using only the statistical errors in the experimental data). The different cases considered are a) soft pomeron b) hard pomeron c) hard pomeron (unevolved) d) ‘intermediate’ pomeron, and then the linear combinations a) + b), a) + c) and a) + d).

with the overall normalization of each left as a free parameter. The results are displayed in the table. The χ^2 of the soft pomeron is rather good and fully compatible with the experimental errors in the data: there are 38 data points, with presumably some correlation in their systematic errors, and our χ^2 is indeed rather low if we combine the statistical and systematic errors for each point in quadrature, but somewhat high if we use only the statistical errors. The fit of the hard pomeron to the data is in contrast very poor, excluding it at the level of at least five standard deviations. Notice that the best-fit value of the normalization is in fact the fraction of the nucleon’s momentum carried by the gluons at the starting scale $\zeta = 0$; the value found in the case of soft boundary conditions is thus in good qualitative agreement with phenomenological expectations, whereas that for the hard boundary condition is typically too small by a factor of two. As a cross-check, we also fitted the linear combination $N_s(F_2^p)^{\text{soft}} + N_h(F_2^p)^{\text{hard}}$, so that both the absolute and relative normalizations of the hard and soft components are left as free parameters. As may be seen from the table, only a very small admixture (less than about 5%) of the hard component is permitted.

We have also determined the corresponding results for an unevolved hard pomeron (again with intercept $\lambda = \frac{1}{2}$). This would presumably be appropriate if the Lipatov equation were somehow to remain valid even when $t \gg t_0$, i.e. in the HERA region.⁹ It

⁹ Amusingly this unevolved hard pomeron may be imitated by adding a negative damping term $-\lambda\partial G/\partial\zeta$ to the left hand side of the gluon evolution equation (8), thereby including $\alpha_s^n \ln^n \frac{1}{x}$ terms in the evolution, and then evolving the soft pomeron from $t = t_0$.

may be seen from the table that in fact this makes very little difference, the improvement in fit as compared to the evolved hard pomeron being at best marginal. Since these are two extreme scenarios, they bracket the intermediate possibility that the value t_0 at which the Lipatov boundary condition should be imposed is somewhere in the middle of the HERA region. In the same spirit we also include an ‘intermediate’ pomeron with intercept $\lambda = 0.35$, since this is supposed to be the minimum value expected from the Lipatov equation [17]. Although this fits a little better than the hard pomeron, it is still clearly excluded.

Finally, we have checked that the χ^2 of the soft pomeron solution is not changed significantly if the value of t_0 is reduced, or if the value of Λ is varied within present experimental uncertainty. Of course, if t_0 is raised too much, so that the data are not yet in the asymptotic region of the soft solution, then χ^2 starts growing and becomes almost as bad as that of the unevolved hard solution: while the data clearly exhibit asymptotic double scaling, this necessarily implies a growth at small x for fixed t which could easily be misinterpreted as evidence for the hard pomeron.

We conclude that there is simply no room for more than a very small admixture of the hard pomeron when $x \gtrsim 10^{-4}$. On the contrary, the data agree surprisingly well with the universal double scaling behaviour which only applies in the case of reasonably soft boundary conditions. These results seem thus to agree with the recent observation [18] that if the integrated k_T in the Lipatov equation is cut-off in the ultraviolet, as required kinematically, λ is very significantly reduced for reasonable values of t , and it becomes very difficult to distinguish the hard perturbative pomeron from the soft nonperturbative one.

Since all existing published data is binned in x and Q^2 , it was necessary when drawing our scaling plots fig. 5 to use all the data in each of the plots, rescaling with the function R_F to ensure that if the data exhibited scaling, they would lie on a single straight line in each of the plots. A rather better test of asymptotic double scaling could be made if the raw data were binned in ρ and σ : plots of $\ln F_2^p(\sigma, \rho)$ at fixed ρ and σ could then be drawn to display both ρ -scaling and σ -scaling. Whereas the approach to a flat (ρ -independent) line of the plots at fixed σ would indicate that asymptotic scaling has been attained, the value of the asymptotic slope of the plots at fixed ρ would be given by the universal value $2\gamma = 12/\sqrt{33 - 6n_f/N_c}$, a parameter-free prediction of perturbative QCD which depends only on the number of colours and flavours.

On the other hand, as much more data becomes available, it should become possible to sharpen the tests of double scaling to the point where the subasymptotic scaling violations at small σ and ρ can be observed and measured; this would be interesting as some of the leading violations (those which are included in (14)) are universal, while the subleading violations could be calculated quite precisely using the known parton distributions at large x and the full evolution equations. It should then be possible to extract (in a rather clean way) α_s from the HERA data. More excitingly, one could also search systematically for scaling violations at large σ and ρ due to new effects such as the hard pomeron or parton recombination.¹⁰ The accurate determination of structure functions at small x will then not only provide a precise and highly nontrivial test of perturbative QCD, but could also be used to search for new physics at small x .

Acknowledgements: We would like to thank M. Arneodo and V. del Duca for discussions, R.G. Roberts and R.K. Ellis for correspondence, and I.J.R. Aitchison, P.H. Damgaard and D.Z. Freedman for encouragement.

¹⁰ Indeed the ρ -scaling plot fig. 5b) does seem to indicate a small (but not as yet statistically significant) rise for $\rho \gtrsim 3$.

References

- [1] J.D. Bjorken, *Phys. Rev.* **179** (1969) 1547.
- [2] H. Georgi and H.D. Politzer, *Phys. Rev.* **D9** (1974) 416;
D. Gross and F. Wilczek, *Phys. Rev.* **D9** (1974) 980.
- [3] G. Parisi, *Proc. 11th Rencontre de Moriond*, ed. J. Tran Thanh Van, ed. Frontières, 1976;
G. Altarelli and G. Parisi, *Nucl. Phys.* **B126** (1977) 298;
G. Altarelli, *Phys. Rep.* **81** (1981) 1.
- [4] ZEUS Collab., *Phys. Lett.* **B316** (1993) 412.
- [5] H1 Collab., *Nucl. Phys.* **B407** (1993) 515.
- [6] A. De Rujula, S.L. Glashow, H.D. Politzer, S.B. Treiman, F. Wilczek and A. Zee, *Phys. Rev.* **D10** (1974) 1649;
see also Yu.L. Dokshitzer, *Sov. Phys. J.E.T.P.* **46** (1977) 641.
- [7] M. Glück and E. Reya, *Phys. Rev.* **D14** (1976) 3034;
F. Martin, *Phys. Rev.* **D19** (1979) 1382.
- [8] T.A. DeGrand, *Nucl. Phys.* **B151** (1979) 485.
- [9] L.V. Gribov, E.M. Levin and M.G. Ryskin *Phys. Rep.* **100** (1983) 1.
- [10] R.K. Ellis, Z. Kunszt, and E.M. Levin, Fermilab-PUB-93/350-T, ETH-TH/93-41, to be published in *Nucl. Phys. B*.
- [11] E. Goursat, *Cours d'Analyse Mathématique, Vol.III*, Gauthier-Villars, 1902.
- [12] H.D.I. Abarbanel, M.L. Goldberger and S.B. Treiman, *Phys. Rev. Lett.* **22** (1969) 500;
P.V. Landshoff, J.C. Polkinghorne and R.D. Short, *Nucl. Phys.* **B28** (1970) 210.
- [13] P.D.B. Collins and F. Gault, *Phys. Lett.* **112B** (1982) 255;
A. Donnachie and P.V. Landshoff, *Nucl. Phys.* **B244** (1984) 322; *Nucl. Phys.* **B267** (1986) 690.
- [14] M. Glück, E. Reya and A. Vogt, *Phys. Lett.* **B306** (1993) 391 and ref. therein.
- [15] L.N. Lipatov, *Sov. Jour. Nucl. Phys.* **23** (1976) 338;
V.S. Fadin, E.A. Kuraev and L.N. Lipatov, *Phys. Lett.* **60B** (1975) 50; *Sov. Phys. JETP* **44** (1976) 443; **45** (1977) 199;
Y.Y. Balitski and L.N. Lipatov, *Sov. Jour. Nucl. Phys.* **28** (1978) 822.
- [16] NMC Collab., *Phys. Lett.* **B295** (1992) 159.
- [17] J.C. Collins and J. Kwiecinski, *Nucl. Phys.* **B316** (1989) 307.
- [18] J.C. Collins and P.V. Landshoff, *Phys. Lett.* **B276** (1992) 196.

Figure Captions

- Fig. 1. Region of validity of the Altarelli-Parisi equation in the (x, t) plane. The disallowed regions are $t < t_0$, where perturbation theory breaks down because $\alpha_s(t)$ becomes too large, and $x \lesssim x_r \exp(-\alpha_s(t_0)^2/\alpha_s(t)^2)$, where recombination effects may become important [9]. The small- x evolution equations may be used above the dashed line. The dotted region with the ? is that in which the Lipatov equation may become applicable.
- Fig. 2. The (ξ, ζ) plane, showing the backward light cone at the point (ξ', ζ') , curves of constant σ (the hyperbolae) and lines of constant ρ .
- Fig. 3. Propagation of G into the ξ - ζ plane; a) soft pomeron, b) hard pomeron. A scatter plot of the NMC and HERA data is superimposed for reference: the two types of crosses are NMC data [16] (taken with 90 GeV and 280 GeV beams respectively), the diamonds are ZEUS data [4], and the squares H1 data [5].
- Fig. 4. Scaling plots of the function $G(\sigma, \rho)$ displayed in fig. 3. The solid lines correspond to fig. 3a) (the soft pomeron) and the dashed lines to fig. 3b) (the hard pomeron); the dotted lines correspond to an unevolved hard initial condition.
- i) $\ln G(\sigma, \rho)$ is plotted versus σ ; the lower line of each pair has $\rho = 1.4$ and the upper one $\rho = 3.2$.
- ii) The rescaled function $R_G(\sigma, \rho)G(\sigma, \rho)$ is plotted versus ρ ; the lower line of each pair has $\sigma = 1.2$ and the upper one $\sigma = 2.1$.
- Fig. 5. Comparison between the experimental data and the predictions for $F_2(\sigma, \rho)$ computed from $G(\sigma, \rho)$ displayed in fig. 4, with normalization now adjusted according to the best-fit values given in the table. The diamonds indicate data from ZEUS [4] and the squares data from H1 [5].
- i) The curves show F_2 computed from G as displayed in fig. 4i) using eqn. (16); the dashed line is a linear fit to the HERA data; a) is the soft pomeron prediction (solid curves of fig. 4i)) and b) is the hard pomeron (dashed curves of fig. 4i)). The subasymptotic data from the NMC are also shown (crosses). The filled points correspond to data with $\rho < 1.4$.
- ii) The curves are now calculated from G as displayed in fig. 4ii), compared to the HERA data rescaled by R_F eq.(17). Again a) is the soft pomeron prediction and b) is the hard pomeron.

This figure "fig1-1.png" is available in "png" format from:

<http://arxiv.org/ps/hep-ph/9405320v3>

This figure "fig2-1.png" is available in "png" format from:

<http://arxiv.org/ps/hep-ph/9405320v3>

This figure "fig1-2.png" is available in "png" format from:

<http://arxiv.org/ps/hep-ph/9405320v3>

This figure "fig2-2.png" is available in "png" format from:

<http://arxiv.org/ps/hep-ph/9405320v3>

This figure "fig1-3.png" is available in "png" format from:

<http://arxiv.org/ps/hep-ph/9405320v3>

This figure "fig2-3.png" is available in "png" format from:

<http://arxiv.org/ps/hep-ph/9405320v3>

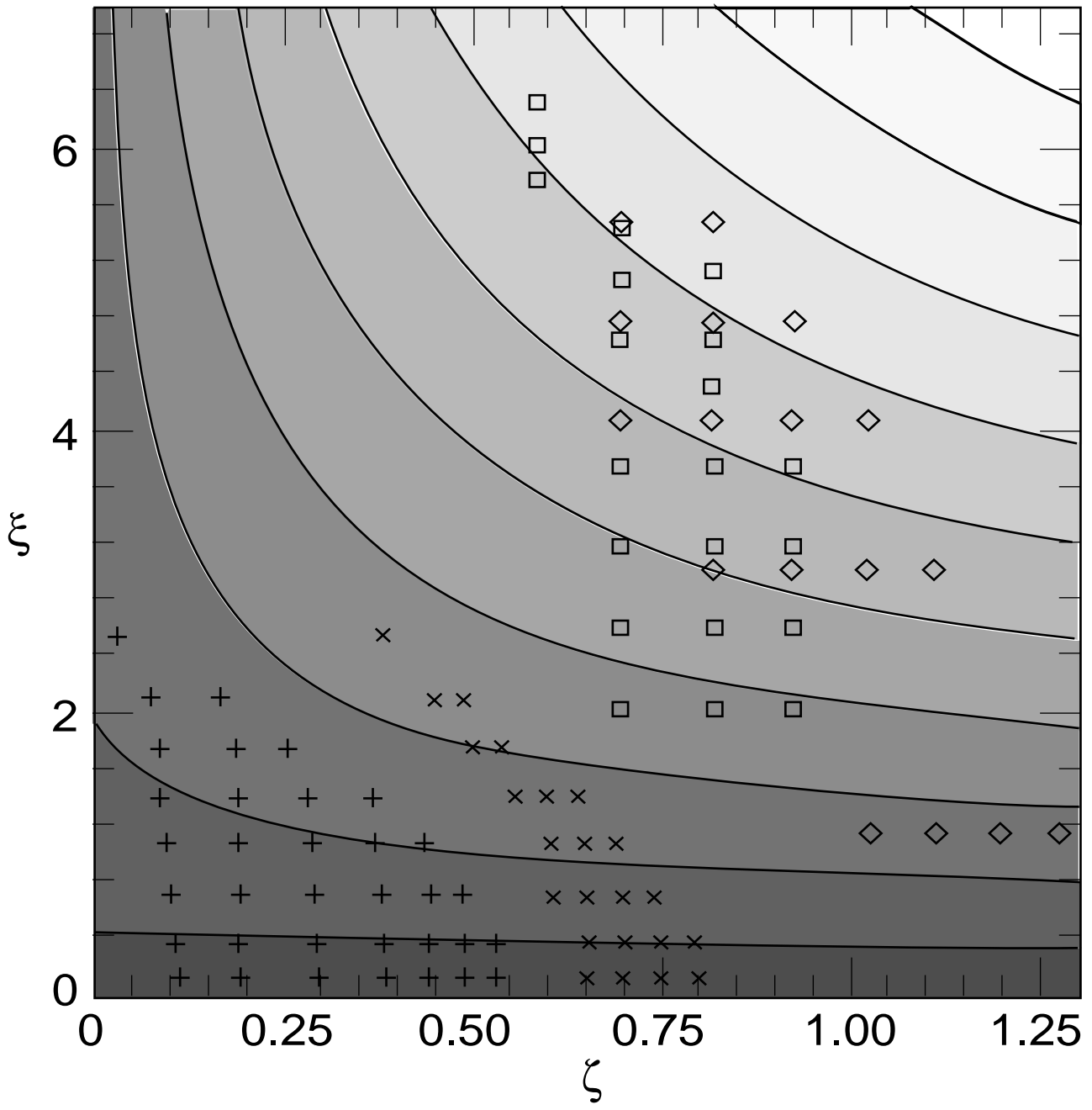


Fig. 3a

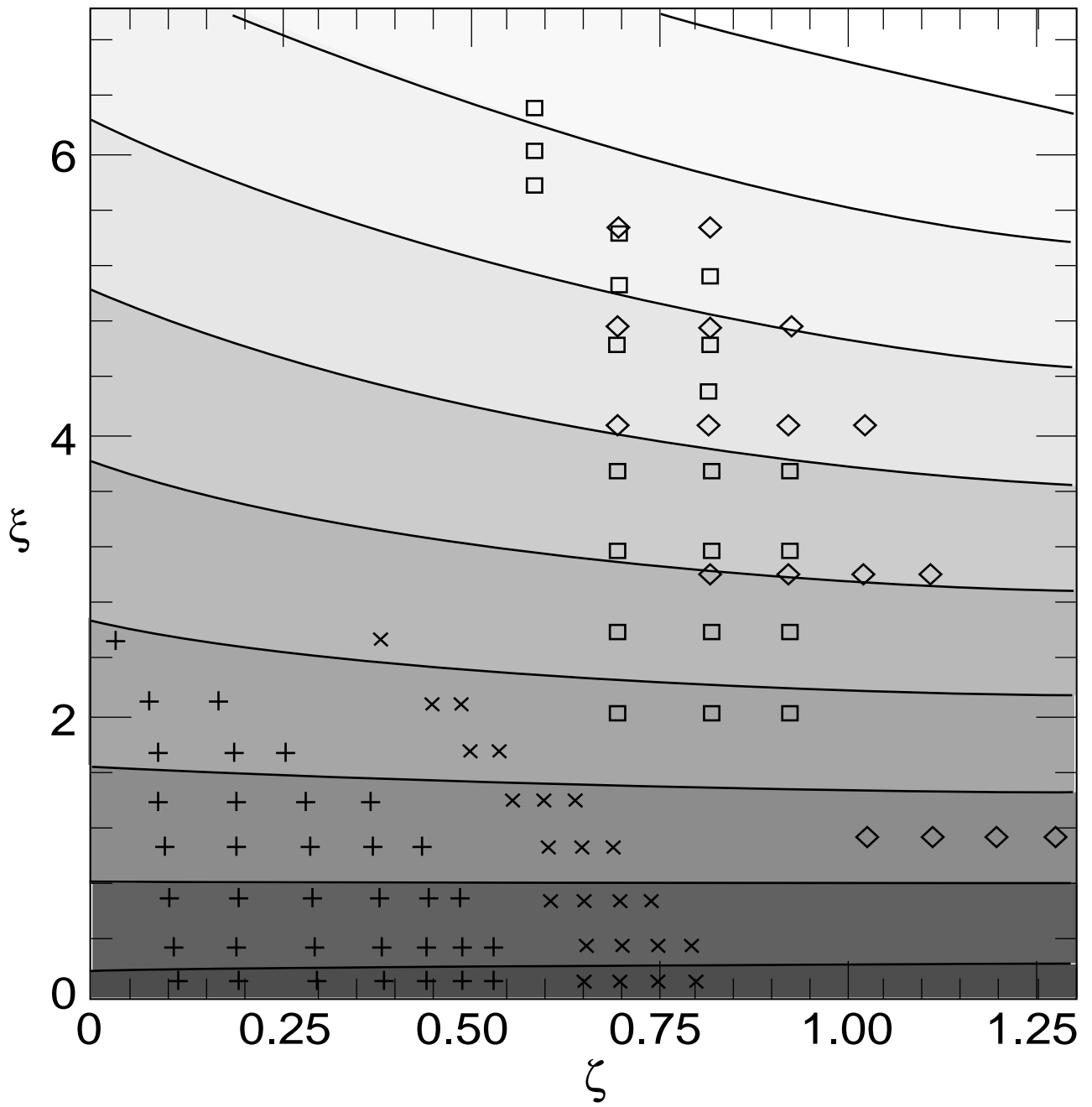


Fig. 3b

This figure "fig1-4.png" is available in "png" format from:

<http://arxiv.org/ps/hep-ph/9405320v3>

This figure "fig2-4.png" is available in "png" format from:

<http://arxiv.org/ps/hep-ph/9405320v3>

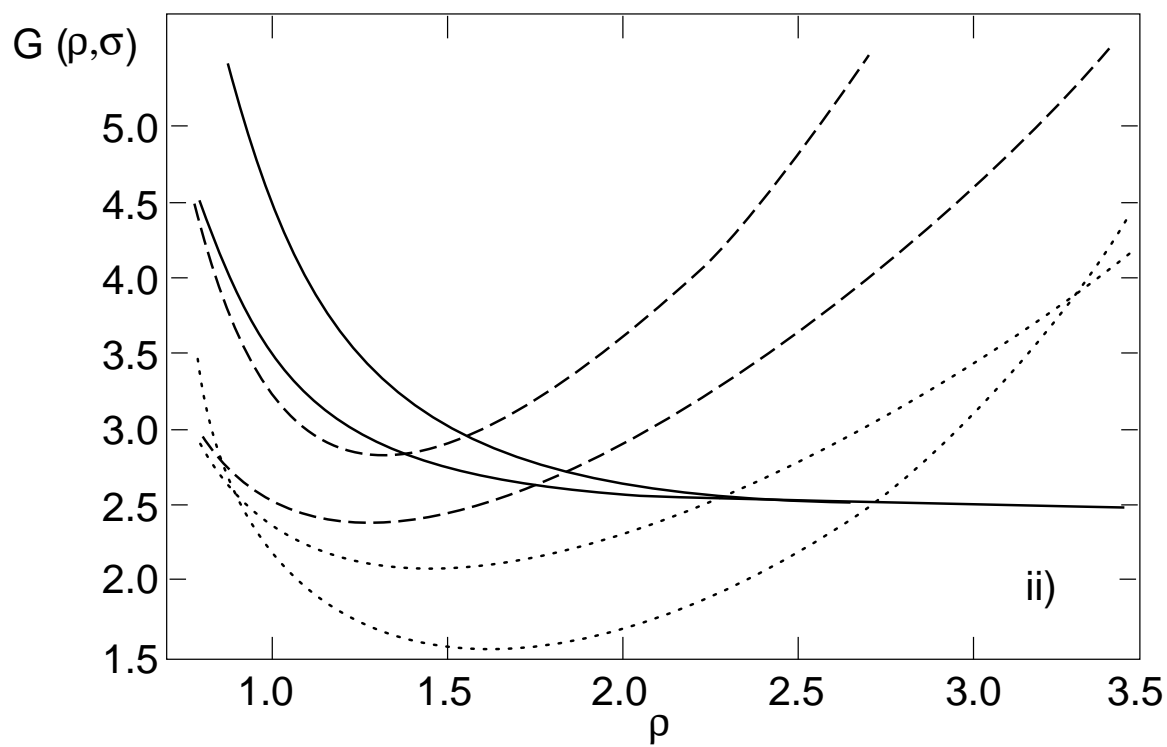
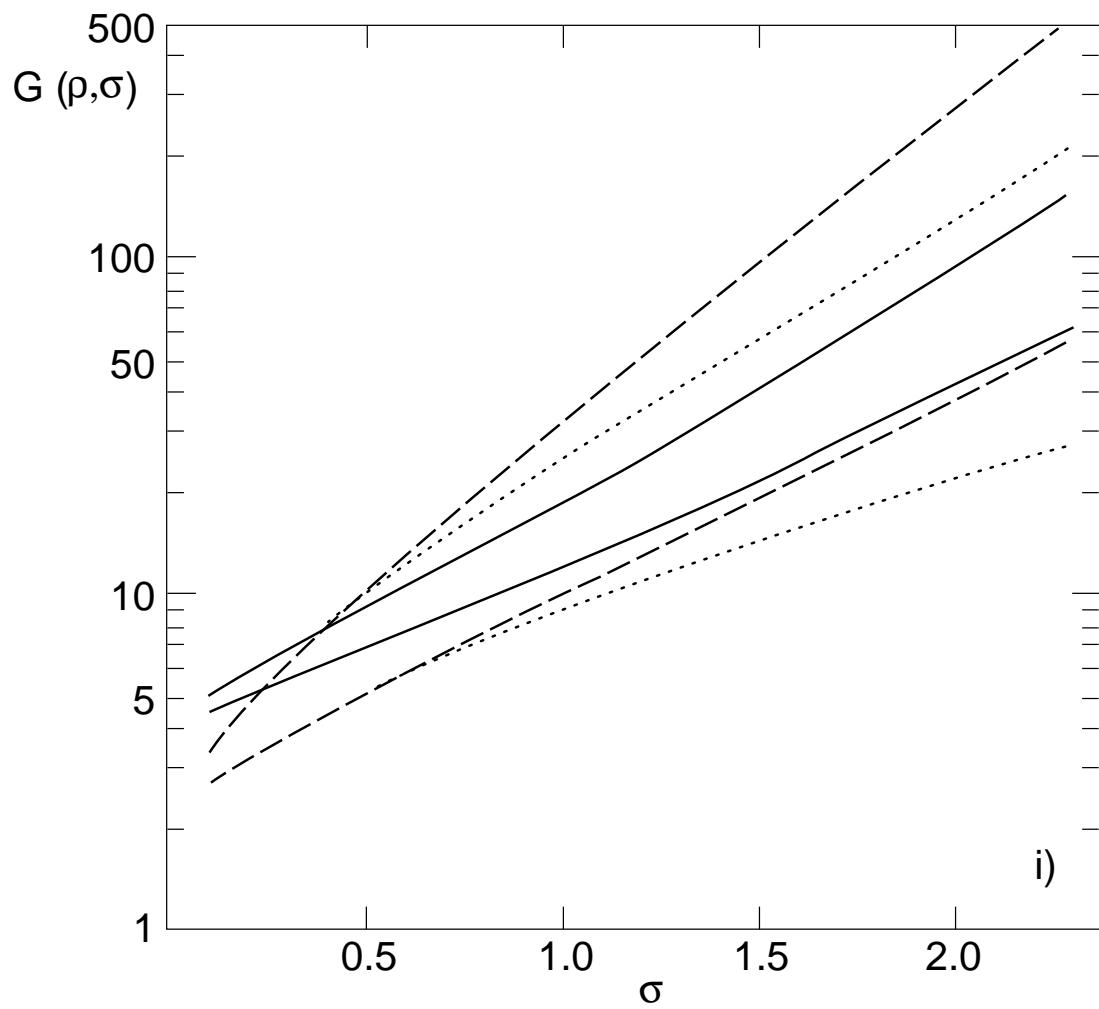


Fig. 4

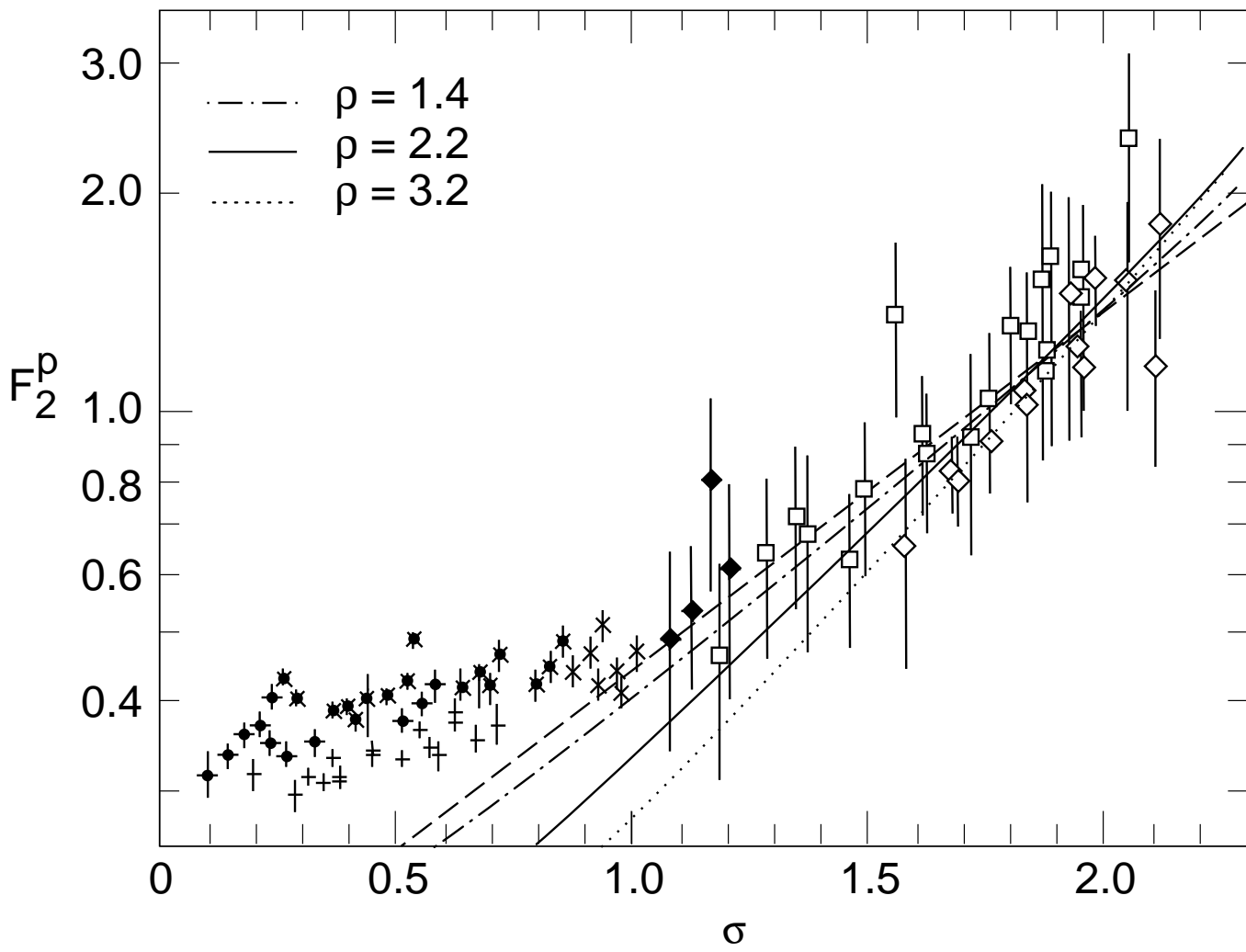


Fig. 5ia

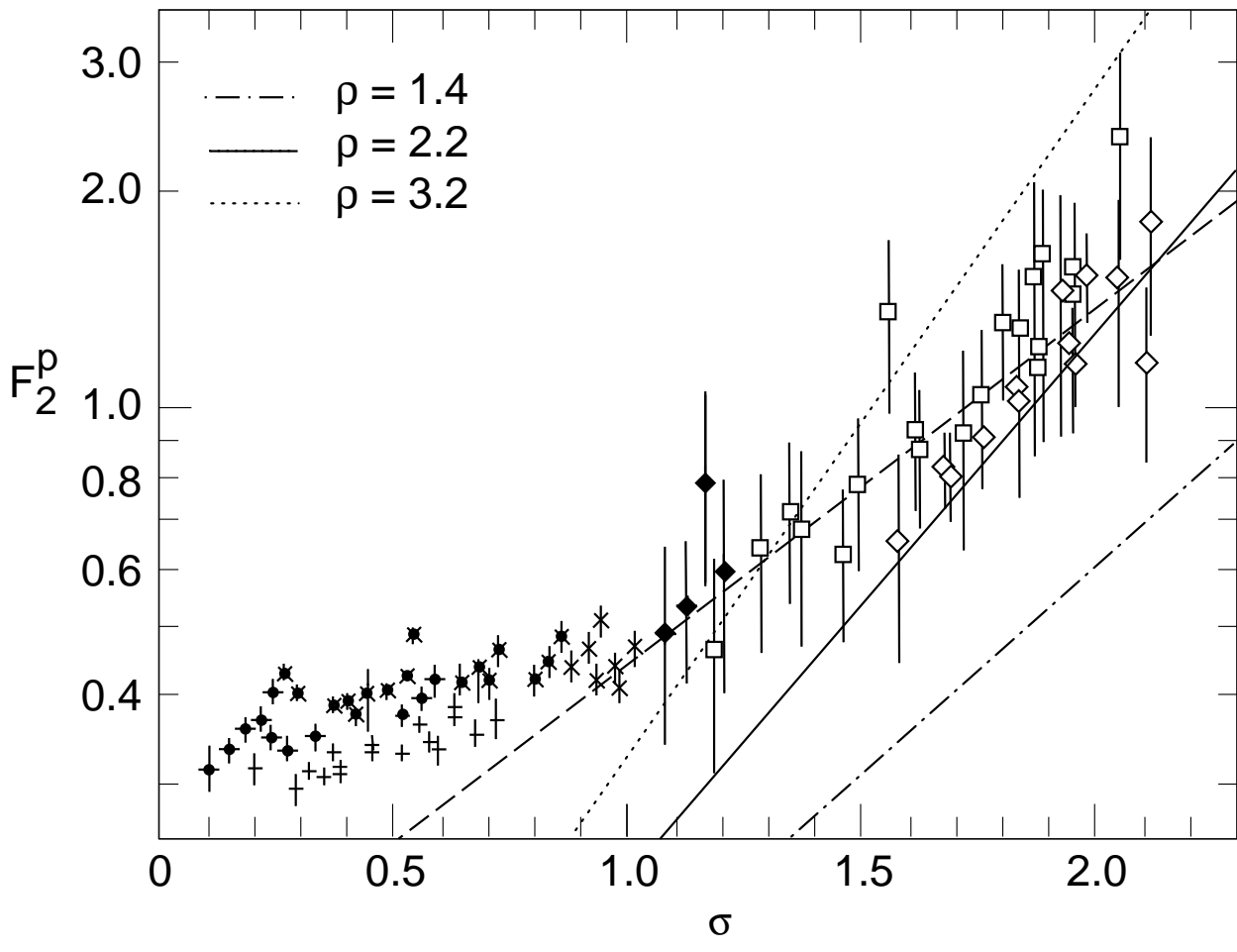


Fig. 5ib

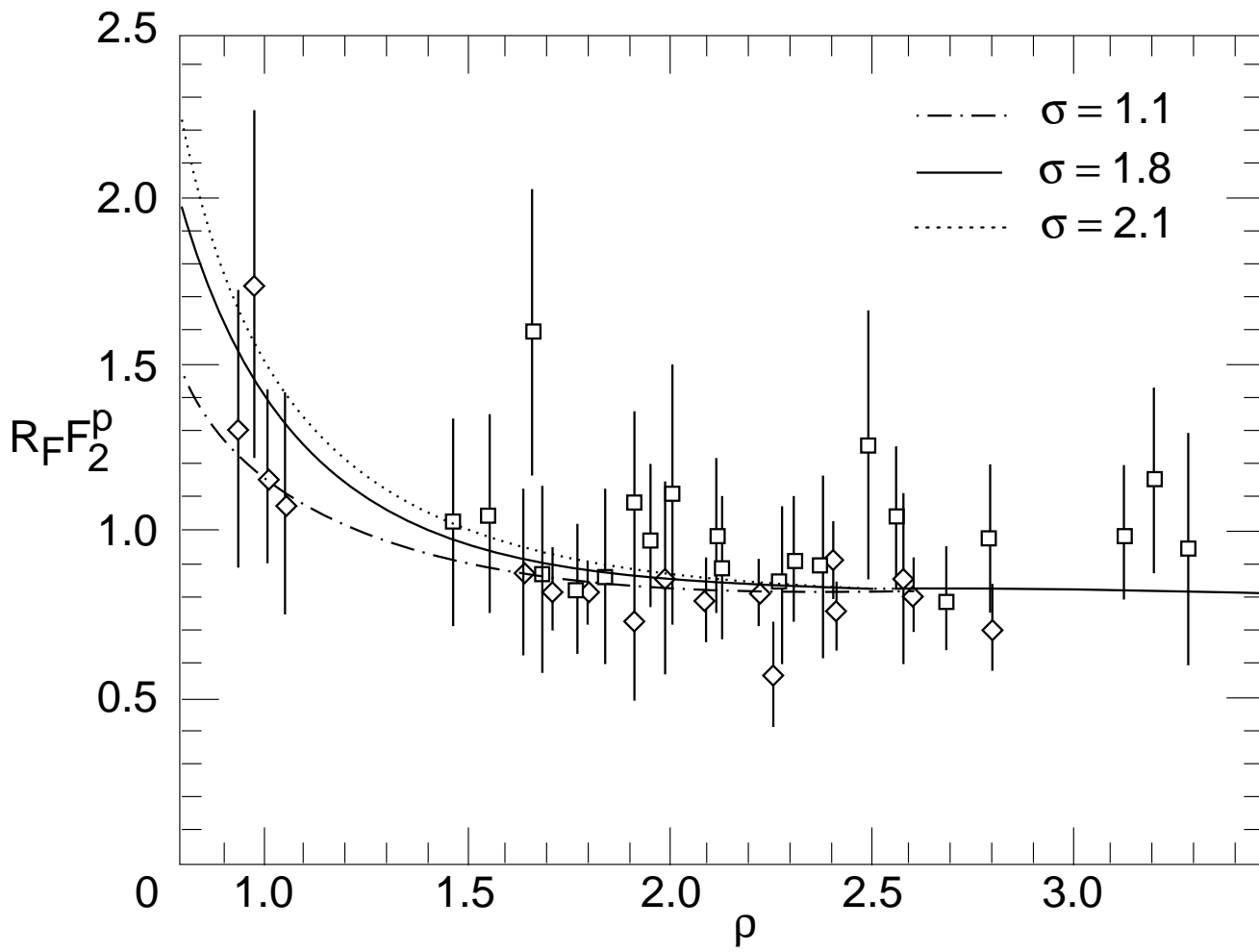


Fig. 5 iia

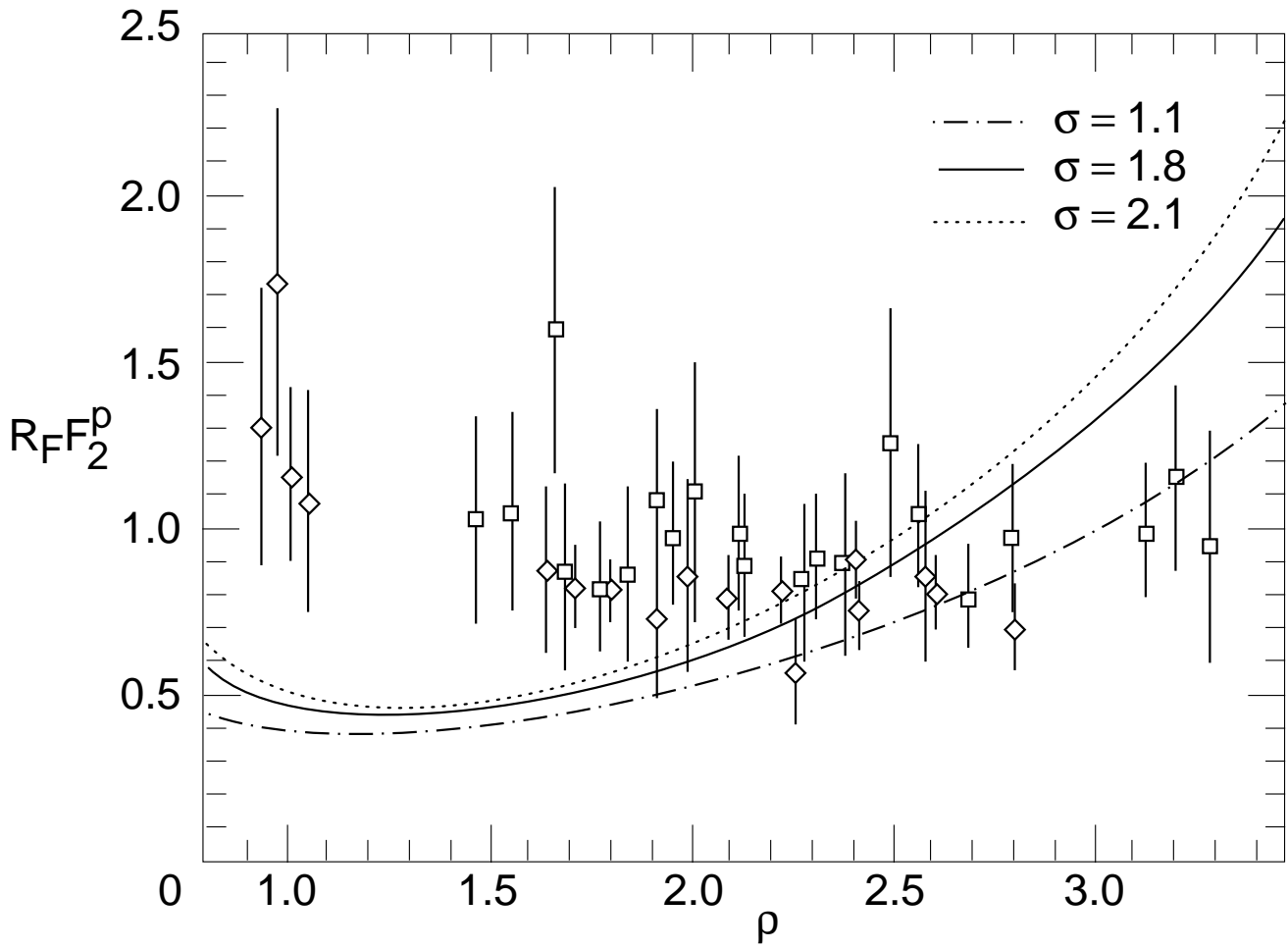


Fig. 5 iib

